Structural Biology and Molecular Biophysics

Absence of electron transfer-associated changes in the time-dependent X-ray free-electron laser structures of the photosynthetic reaction center

Gai Nishikawa, Yu Sugo, Keisuke Saito, Hiroshi Ishikita

Department of Applied Chemistry, The University of Tokyo, 7-3-1 Hongo, Bunkyo-ku, Tokyo 113-8654, Japan • Research Center for Advanced Science and Technology, The University of Tokyo, 4-6-1 Komaba, Meguro-ku, Tokyo 153-8904, Japan

Reviewed Preprint

Revised by authors after peer review.

About eLife's process

Reviewed preprint version 3
September 4, 2023 (this version)

Reviewed preprint version 2
August 8, 2023

Reviewed preprint version 1
July 14, 2023

Sent for peer review
May 14, 2023

Posted to bioRxiv
May 3, 2023

Abstract

Using the X-ray free-electron laser (XFEL) structures of the photosynthetic reaction center from *Blastochloris viridis* that show light-induced time-dependent structural changes [Dods, R.et al. (2021) Nature *589*, 310-314], we investigated time-dependent changes in the energetics of the electron transfer pathway, considering the entire protein environment of the protein structures and titrating the redox active sites in the presence of all fully equilibrated titratable residues. In the dark and charge-separation intermediate structures, the calculated redox potential (E_m) values for the accessory bacteriochlorophyll and bacteriopheophytin in the electron-transfer active branch (B_L and H_L) are higher than those in the electron-transfer inactive branch (B_M and H_M). However, the stabilization of the $[P_LP_M]^{\bullet+}H_L^{\bullet-}$ state owing to protein reorganization is not clearly observed in the $E_m(H_L)$ values in the charge-separated 5-ps ($[P_LP_M]^{\bullet+}H_L^{\bullet-}$ state) structure. Furthermore, the expected chlorin ring deformation upon formation of $H_L^{\bullet-}$(saddling mode) is absent in the H_L geometry of the original 5-ps structure. These findings suggest that there is no clear link between the time-dependent structural changes and the electron transfer events in the XFEL structures.

eLife assessment

The manuscript describes **valuable** theoretical calculations focusing on the structural changes in the photosynthetic reaction center postulated by others based on time-resolved crystallography using X-ray free-electron laser (XFEL) (Dods et al., Nature, 2021). The authors provide **solid** arguments that calculated changes in redox potential Em and deformations using the XEFL structures may reflect experimental errors rather than real structural changes.

Introduction

Photosynthetic reaction centers from purple bacteria (PbRC) are heterodimeric reaction centers, which are formed by the protein subunits L and M (**Figure 1**). In PbRC from *Blastochloris viridis*, the electronic excitation of the bacteriochlorophyll *b* (BChl*b*) pair, $[P_LP_M]$, leads to electron transfer to accessory BChl*b*, B_L, followed by electron transfer via bacteriopheophytin *b* (BPheo*b*), H_L, to menaquinone, Q_A, along the electron-transfer active L branch (A branch) [1]. Electron transfer further proceeds from Q_A to ubiquinone, Q_B, which is coupled with proton transfer via charged and polar residues in the Q_B binding region [2]. Although the counterpart M branch (B branch) is essentially electron-transfer inactive, mutations of the Phe-L181/Tyr-M208 pair to tyrosine/phenylalanine lead to an increase in the yield of $[P_LP_M]^{\bullet+}H_M^{\bullet-}$ formation (~30%), which suggests that these residues are responsible for the energetic asymmetry in the electron transfer branches (e.g., [3]). The anionic states $B_L^{\bullet-}$, $H_L^{\bullet-}$, and $Q_A^{\bullet-}$ form in ~3.5 ps, ~5 ps, and ~200 ps upon the formation of the electronically excited $[P_LP_M]^*$ state, respectively [4]. The anionic state formation induces not only reoriganization of the protein environment [5] but also out-of-plane distortion of the chlorin ring [6]. Indeed, two distinct conformations of $H_L^{\bullet-}$ were reported in spectroscopic studies of PbRC from *Rhodobacter sphaeroides* [7].

Recently, using the X-ray free electron laser (XFEL), light-induced electron density changes and structural changes of PbRC were analyzed at 1 ps, 5 ps, 20 ps, 300 ps, and 8 μs upon the electronic excitation of $[P_LP_M]$ at 960 nm [8]: the 1 ps XFEL structure represents the $[P_LP_M]^*$ state, the 5 ps and 20 ps XFEL structures represent the charge-separated $[P_LP_M]^{\bullet+}H_L^{\bullet-}$ state, and the 300 ps and 8 μs XFEL structures represent the charge-separated $[P_LP_M]^{\bullet+}Q_A^{\bullet-}$ state. According to Dods et al. [8], these XFEL structures revealed how the charge-separation process was stabilized by protein conformational dynamics. However, the conclusions drawn from these XFEL structures are based on data with limited resolution. Specifically, 8 out of 9 XFEL structures have a resolution of 2.8 Å (atomic coordinates from PDB codes: 5O4C, 6ZI4, and 6ZI5 for dataset a and 6ZHW, 6ZID, 6ZI6, 6ZI9, and 6ZIA for dataset b) [8]. The data statistics may indicate that the high-resolution range of some XFEL datasets exhibits high levels of noise (e.g., low $CC_{1/2}$). These observations raise concerns about the reliable comparison of subtle conformational changes among these XFEL structures. Hence, caution must be exercised when interpreting these XFEL structures in terms of their ability to accurately capture relevant conformational changes.

Here, we investigated how the redox potential (E_m) values of the BChl*b* and BPheo*b* cofactors for one-electron reduction change as electron transfer proceeds using the dark (0 ps), 1 ps, 5 ps, 20 ps, 300 ps, and 8 μs XFEL structures, solving the linear Poisson-Boltzmann equation, and considering the protonation states of all titratable sites in the entire protein. Structural changes (e.g., side-chain orientation) in the protein environment can be analyzed in the E_m shift, as E_m is predominantly determined by the sum of the electrostatic interactions between the redox-active site and all other groups (i.e., residues and cofactors) in the protein structure. Subtle structural changes of the BChl*b* and BPheo*b* chlorin rings, which may not be pronounced even in the E_m shift [6], can be analyzed in the out-of-plane distortion of the chlorin rings using a normal-coordinate structural decomposition (NSD) analysis [9, 10] with a combination of a quantum mechanical/molecular mechanical (QM/MM) approach in the entire PbRC protein environment.

Methods

Coordinates and atomic partial charges

The atomic coordinates of PbRC from *Blastochloris viridis* were taken from the XFEL structures determined at 0 ps (dark state; PDB code 5O4C for dataset a and 5NJ4 for dataset b), 1 ps ($[P_LP_M]^*$ state; PDB code, 6ZHW for dataset b), 5 ps ($[P_LP_M]^{\bullet+}H_L^{\bullet-}$ state; PDB code, 6ZI4 for dataset a and

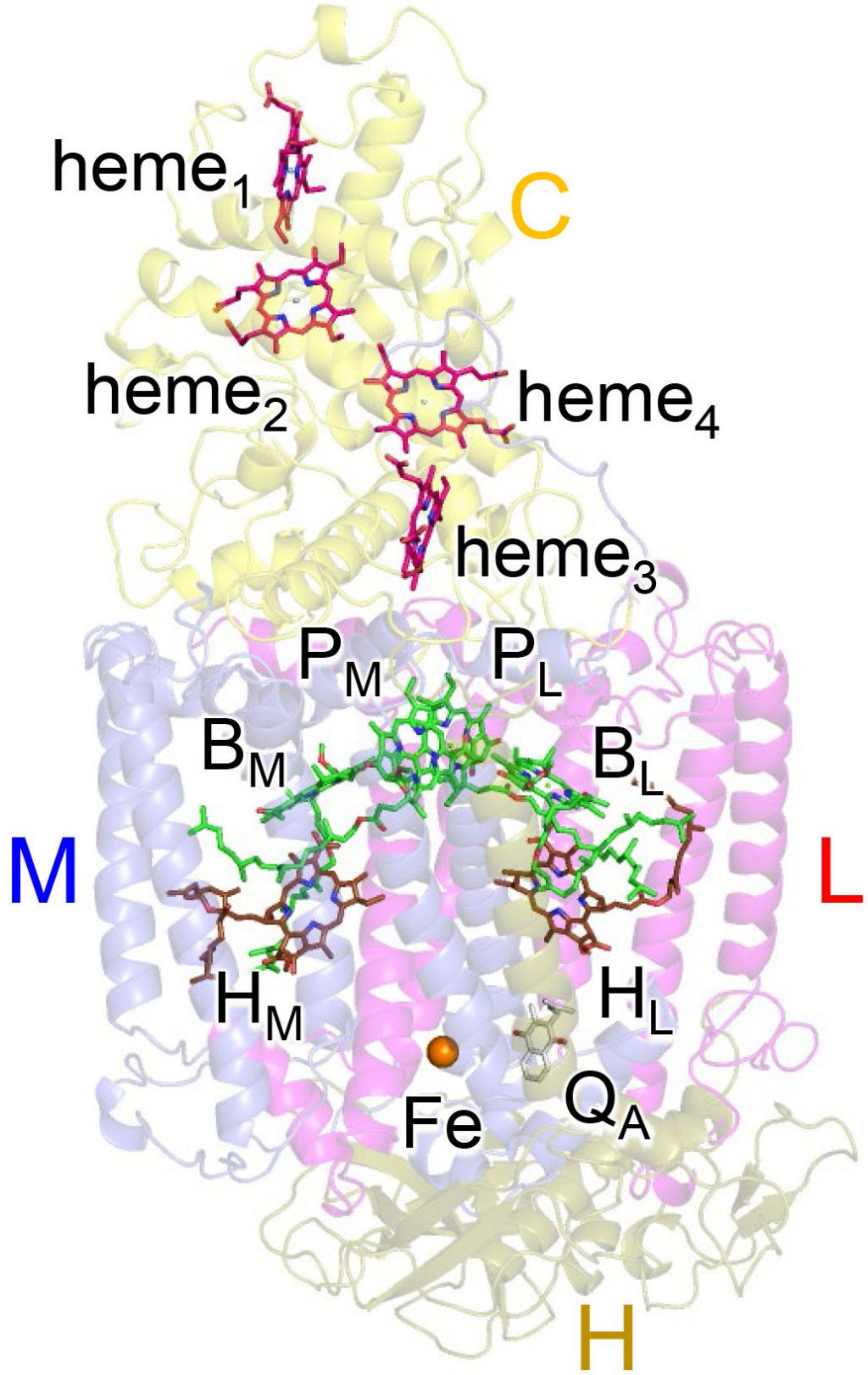

Figure 1.

Electron transfer pathways along the L- and M-branches in PbRC from *Blastochloris viridis*. The PbRC is composed of the L (red), M (blue), H (gold), and C (yellow) subunits. [P_LP_M]: BChl*b* pair; B_L and B_M: accessory BChl*b*; H_L and H_M: BPheo*b*; Q_A: primary quinone (menaquinone); Fe: non-heme Fe complex.

6ZID for dataset b), 20 ps ($[P_LP_M]^{\bullet+}H_L^{\bullet-}$ state; PDB code, 6ZI6 for dataset b), 300 ps ($[P_LP_M]^{\bullet+}Q_A^{\bullet-}$ state; PDB code, 6ZI5 for dataset a and 6ZI9 for dataset b), and 8 μs ($[P_LP_M]^{\bullet+}Q_A^{\bullet-}$ state; PDB code, 6ZIA for dataset b). Atoms with 30% occupancy for the photoactivated state [8] were used wherever present. Hydrogen atoms were generated and energetically optimized with CHARMM [11]. The atomic partial charges of the amino acids were obtained from the all-atom CHARMM22 [12] parameter set. For diacylglycerol, the Fe complex [13], and menaquinone [14], the atomic charges were adopted from previous studies. The atomic charges of BChl*b* and BPheo*b* (BChl*b*, BChl$b^{\bullet+}$, BChl$b^{\bullet-}$, BPheo*b*, and BPheo$b^{\bullet-}$) were determined by fitting the electrostatic potential in the neighborhood of these molecules using the RESP procedure [15] (Tables S1). The electronic densities were calculated after geometry optimization using the DFT method with the B3LYP functional and 6-31G** basis sets in the JAGUAR program [16]. For the atomic charges of the nonpolar CH_n groups in the cofactors (e.g., the phytol chains of BChl*b* and BPheo*b* and the isoprene side chains of quinone), a value of +0.09 was assigned to nonpolar H atoms.

Calculation of E_m: solving the linear Poisson-Boltzmann equation

The E_m values in the protein were determined by calculating the electrostatic energy difference between the two redox states in a reference model system. This was achieved by solving the linear Poisson-Boltzmann equation with the MEAD program [17] and using E_m(BChl*b*) = –665 mV and E_m(BPheo*b*) = –429 mV (based on E_m(BChl*b*) = –700 mV and E_m(BPheo*b*) = –500 mV for one-electron reduction measured in dimethylformamide [18,19]), considering the solvation energy difference). The $E_m(Q_A)$ value was calculated, using the reference E_m value of –256 mV versus NHE for menaquinone-2 in water [20]. The difference in the E_m value of the protein relative to the reference system was added to the known E_m value. To account for the ensemble of protonation patterns, a Monte Carlo method with Karlsberg was used for sampling [21]. The linear Poisson-Boltzmann equation was solved using a three-step grid-focusing procedure with resolutions of 2.5 Å, 1.0 Å, and 0.3 Å. Monte Carlo sampling provided the probabilities $[A_{ox}]$ and $[A_{red}]$ of the two redox states of molecule *A*, and E_m was evaluated using the Nernst equation. A bias potential was applied to ensure an equal amount of both redox states ($[A_{ox}] = [A_{red}]$), thus determining the redox midpoint potential as the resulting bias potential. To ensure consistency with previous computational results, we used identical computational conditions and parameters as previous studies (e.g., [13]), performing all computations at 300 K, pH 7.0, and an ionic strength of 100 mM. The dielectric constants were set to 4 for the protein interior and 80 for water.

QM/MM calculations

We employed the restricted DFT method for describing the closed-shell electronic structure and the unrestricted DFT method for the open-shell electronic structure with the B3LYP functional and LACVP* basis sets using the QSite [22] program. To neutralize the entire system, counter ions were added randomly around the protein using the Autoionize plugin in VMD [23]. In the QM region, all atom positions were relaxed in the QM region, while the H-atom positions were relaxed in the MM region. The QM regions were defined as follows: for the BChl*b* pair $[P_LP_M]$: the side chains of the ligand residues (His-L173 and His-M200) and H-bod partners (His-L168, Tyr-M195, and Thr-L248); for accessory BChl*b*: B_L/B_M and the side chain of the ligand residue (His-L153 for B_L/His-M180 for B_M); for BPheo*b*: H_L/H_M.

NSD analysis

To analyze the out-of-plane distortions of chlorin rings, we employed an NSD procedure with the minimal basis approximation, where the deformation profile can be represented by the six lowest-frequency normal modes, i.e., ruffling (B_{1u}), saddling (B_{2u}), doming (A_{2u}), waving ($E_{g(x)}$ and $E_{g(y)}$), and propellering (A_{1u}) modes [9,10]. The NSD analysis was performed in the following three steps, as performed previously [6]. First, the atomic coordinates of the Mg-substituted macrocycle were extracted from the crystal (or QM/MM optimized) structure. Second, the extracted coordinates were superimposed on the reference coordinates of the macrocycle. The

superimposition is based on a least-square method, and the mathematical procedure is described in Ref. [24]. Finally, the out-of-plane distortion in the superimposed coordinates was decomposed into the six lowest-frequency normal modes by the projection to the reference normal mode coordinates as

$$d^{\Gamma} = \sum_{i=1}^{N} \Delta z_i (n_z^{\Gamma})_i \,, \qquad \text{(Eq.1)}$$

where d^{Γ} represents the distortion component of the mode Γ (i.e., Γ = B_{1u}, B_{2u}, A_{2u}, $E_{g(x)}$, $E_{g(y)}$, or A_{1u}), Δz_i is the z-component of the superimposed coordinates in the ith heavy atom, and $(n_z^{\Gamma})_i$ is the z-component of the normalized eigenvector of the reference normal mode Γ in the ith heavy atom. N represents the number of heavy atoms. See ref. [6] for further details.

Results and discussion

Energetically asymmetric electron transfer branches

The XFEL structures show that the E_m values for B_L are ~50 mV higher than those for B_M, which facilitates the formation of the charge-separated $[P_LP_M]^{\bullet+}B_L^{\bullet-}$ state and thereby electron transfer along the L-branch (**Figures 2** and **3**). As the E_m profile is substantially consistent with the E_m profile for PbRC from *Rhodobacter sphaeroides* [13], it seems plausible that the charge-separated $[P_LP_M]^{\bullet+}B_L^{\bullet-}$ and $[P_LP_M]^{\bullet+}H_L^{\bullet-}$ states in the active L-branch are energetically lower than the $[P_LP_M]^{\bullet+}B_M^{\bullet-}$ and $[P_LP_M]^{\bullet+}H_M^{\bullet-}$ states in the inactive M-branch, respectively, as demonstrated in QM/MM/PCM calculations [25]. Indeed, the calculated E_m values are largely correlated with the LUMO levels calculated using a QM/MM approach, as suggested previously (coefficient of determination R^2 = 0.98, Figure S1). The $E_m(H_L)$ value of –597 mV is in line with the experimentally estimated value of ca. –600 mV for H_L in PbRC from *Blastochloris viridis* [26].

Among the L/M residue pairs, the Phe-L181/Tyr-M208 pair contributes to $E_m(B_L) > E_m(B_M)$ most significantly (27 mV), facilitating L branch electron transfer, as suggested in theoretical studies [27] (**Table 1**, **Figure 3a**). This result is also consistent with the contribution of the Phe-L181/Tyr-M210 pair to the difference between $E_m(B_L)$ and $E_m(B_M)$, which was the largest in PbRC from *Rhodobacter sphaeroides* [28] (26 mV [13]). The Asn-L158/Thr-M185 pair also contributes to the difference between $E_m(B_L)$ and $E_m(B_M)$ (11 mV, **Table 1**), as does the Val-L157/Thr-M186 pair in PbRC from *Rhodobacter sphaeroides* (22 mV [13]).

The E_m values for H_L are ~50 mV higher than those for H_M in the dark state and [5 ps and 300 ps] XFEL structures, as observed in $E_m(B_L)$ and $E_m(B_M)$ (**Figure 2a,c,e**). However, the E_m difference decreases to ~25 mV in the [1 ps, 20 ps, and 8 μs] XFEL structures (**Figure 2b,d,f**), which implies that the dark state and [5 ps and 300 ps] XFEL structures are distinct from the [1 ps, 20 ps, and 8 μs] XFEL structures (see below). Below, we discuss the dark state structure if not otherwise specified.

The Ala-L120/Asn-M147 pair contributes to $E_m(H_L) > E_m(H_M)$ most significantly (38 mV) (**Table 2**, Figure S2). However, this holds true only for PbRC from *Blastochloris viridis*, as Asn-M147 is replaced with alanine (Ala-M149) in PbRC from *Rhodobacter sphaeroides*. The Asp-L218/Trp-M252 pair decreases $E_m(H_M)$ with respect to $E_m(H_L)$, thereby contributing to $E_m(H_L) > E_m(H_M)$ (20 mV) (**Table 2**, Figure S2). Arg-L103 orients toward the protein interior, whereas Arg-M130 orients toward the protein exterior (Figure S2), which contributes to $E_m(H_L) > E_m(H_M)$ (17 mV) (**Table**

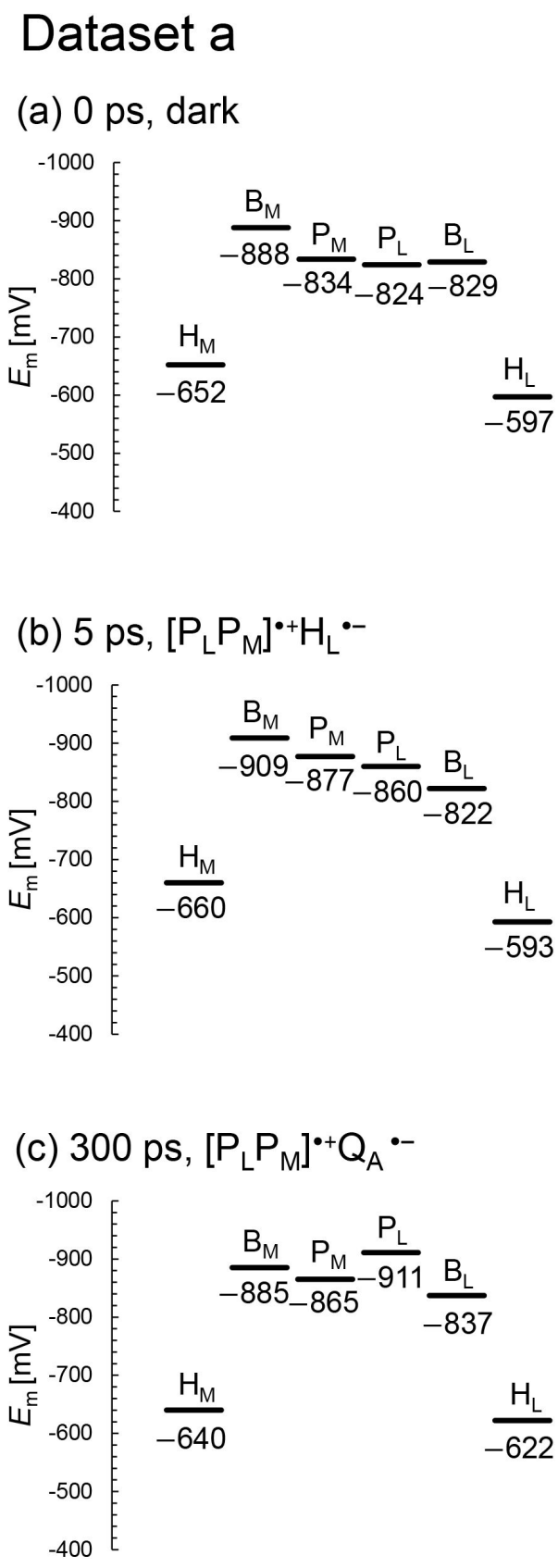

Figure 2.

E_m profiles along the L- and M-branches in the XFEL structures for dataset a. (a) 0 ps. (b) 5 ps. (c) 300 ps.

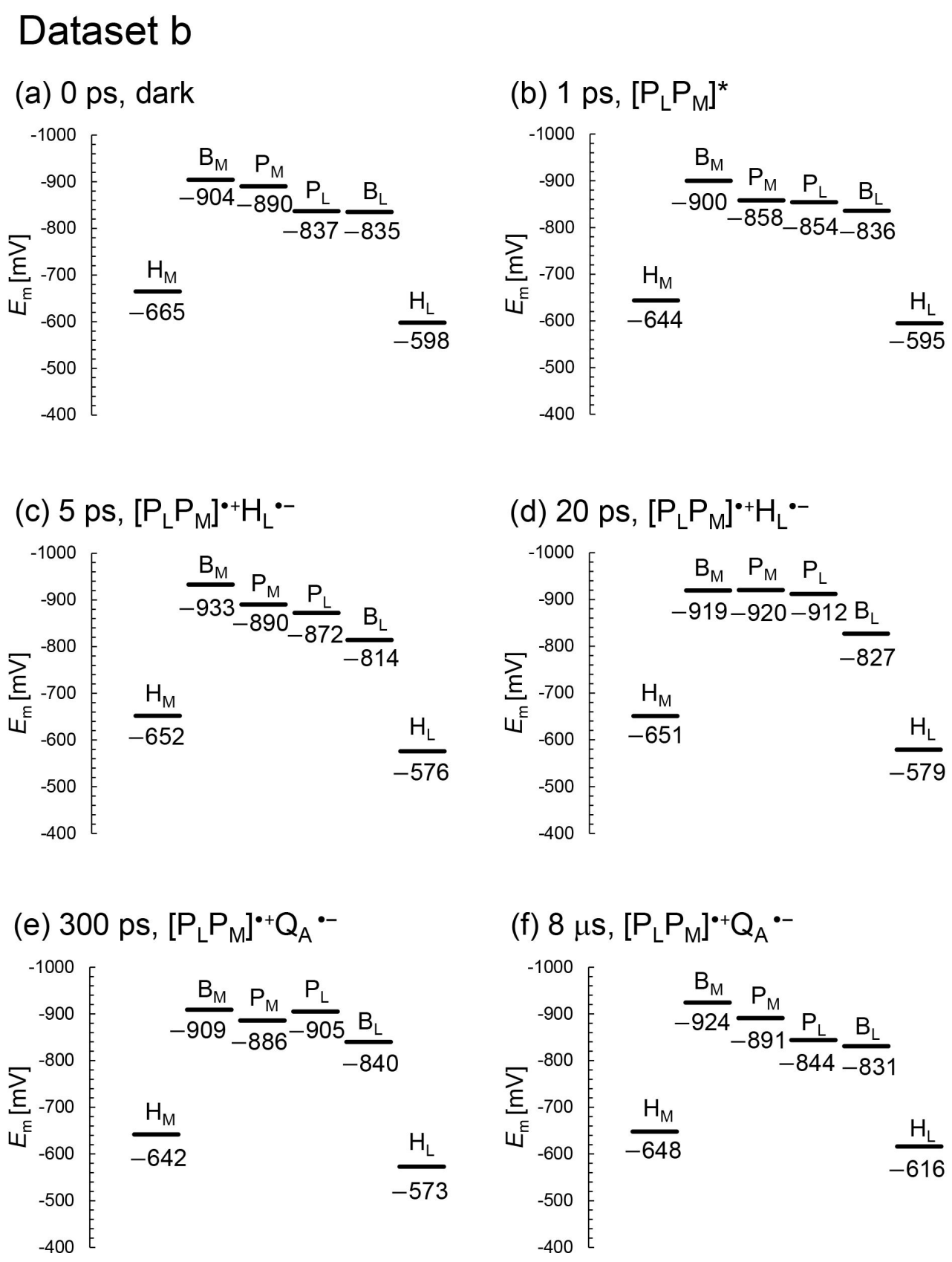

Figure 3.

E_m profiles along the L- and M-branches in the XFEL structures for dataset b. (a) 0 ps. (b) 1 ps. (c) 5 ps. (d) 20 ps. (e) 300 ps. (f) 8 μs.

Subunit L	$E_m(B_L)$	$E_m(B_M)$	Subunit M	$E_m(B_L)$	$E_m(B_M)$	Difference
Phe-L181	0	17	Tyr-M208	39	-3	25
His-L144	-8	-2	Glu-M171	-14	-45	25
Asn-L158	5	-6	Thr-M185	-3	-4	12

Table 1.

Contributions of the L/M residue pairs that are responsible for $E_m(B_L) > E_m(B_M)$ (more than 10 mV) in the dark-state structure (mV). Difference: [contribution of subunit L to $E_m(B_L)$] + [contribution of subunit M to $E_m(B_L)$] – [contribution of subunit L to $E_m(B_M)$] – [contribution of subunit M to $E_m(B_M)$].

2). Ser-M271 forms an H-bond with Asn-M147 near H_M (**Figure 3b**). Thus, the contribution of Ser-M271 to $E_m(H_L)$ is large, although this residue is replaced with alanine (Ala-M273) in PbRC from *Rhodobacter sphaeroides*.

Relevance of structural changes observed in XFEL structures

According to Dods et al., the 5-ps and 20-ps structures correspond to the charge-separated $[P_LP_M]^{\bullet+}H_L^{\bullet-}$ state [8]. If this is the case, $E_m(H_L)$ is expected to be exclusively higher in the 5-ps and 20-ps structures than in the other XFEL structures due to the stabilization of the $[P_LP_M]^{\bullet+}H_L^{\bullet-}$ state by protein reorganization. In dataset a, the $E_m(H_L)$ value is only 4 mV higher in the 5-ps structure than in the dark structure (**Figure 5a**). In dataset b, the $E_m(H_L)$ value is ~20 mV higher in the 5- and 20-ps structures than in the dark structure (**Figure 5b**). However, the $E_m(H_L)$ value is 25 mV higher in the 300-ps structure than in the dark structure. **Tables 3** and **4** show the residues that contribute to the slight increase in $E_m(H_L)$ most significantly in the 5- and 20-ps structures. Most of these residues were in the region where Dods et al. specifically performed multiple rounds of partial occupancy refinement (e.g., 153–178, 190, 230 and 236–248 of subunit L and 193–221, 232, 243– 253, 257–266 of subunit M) [8]. In dataset b (**Table 4**), which has more data points than dataset a (**Table 3**), the contributions of these residues to $E_m(H_L)$ often fluctuate (e.g., upshift/downshift followed by downshift/upshift) at different time intervals (e.g., 1 to 5 ps, 5 to 20 ps, and 20 to 300 ps). This result suggests that the structural differences among the XFEL structures are not related to the actual time course of charge separation. Furthermore, the $E_m(H_M)$ value in the inactive M branch is also ~15 mV higher in the 5- and 20-ps structures than in the dark structure (**Figure 5b**). These results suggest that the ~20 mV higher $E_m(H_L)$ value in the 5- and 20-ps structures is not specifically due to the formation of the $[P_LP_M]^{\bullet+}H_L^{\bullet-}$ state. Thus, the stabilization of the $[P_LP_M]^{\bullet+}H_L^{\bullet-}$ state owing to protein reorganization is not clearly observed in the $E_m(H_L)$ values.

A normal-coordinate structural decomposition (NSD) analysis [9, 10] of the out-of-plane distortion of the chlorin ring is sensitive to subtle structural changes in the chlorin ring, which are not distinct in the E_m changes [6]. QM/MM calculations indicate that $H_L^{\bullet-}$ formation induces the saddling mode in the chlorin ring, which describes the movement of rings I and III being in the opposite direction to the movement of rings II and IV along the normal axis of the chlorin ring (**Tables 5** and **6**). However, (i) in the XFEL structures, the saddling mode of H_L remains practically unchanged in dataset a during electron transfer (**Figure 6** and Tables S2 and S3). In dataset b, the saddling mode of H_L is induced most significantly at 1 ps, which does not correspond to the charge-separated $[P_LP_M]^{\bullet+}H_L^{\bullet-}$ state (**Figure 7**). (ii) In addition, the ruffling mode is more pronounced than the saddling mode in H_L (**Figure 7**), which suggests that the observed deformation of H_L is not directly associated with the reduction of H_L.

One might argue that the loss of the link between the formation of the charge-separated state and the $E_m(H_L)$ change (**Figure 5**) is not due to experimental errors but rather represents the actual ps-timescale phenomena during the primary charge-separation reactions (e.g., Dods et al. noted that “the primary electron-transfer step to H_L is more rapid than conventional Marcus theory” [8]). However, even if this were the case, this hypothesis regarding the relevance of the XFEL structures to the electron-transfer events could be further explored by examining the changes in $E_m(Q_A)$ among the XFEL structures, considering the relatively slow electron-transfer step to Q_A that allows sufficient protein relaxation to occur (e.g., Dods et al. stated that “the electron-transfer step to Q_A has a single exponential decay time of 230 ± 30 ps, consistent with conventional Marcus theory” [8]). That is, if the $E_m(Q_A)$ values are not higher in the 300-ps and 8-μs structures than in the other structures, it suggests that significant experimental errors exist, rendering the XFEL structures irrelevant to the electron transfer events. Consistent with this perspective, the present results demonstrate that the $E_m(Q_A)$ values in the 300-ps and 8-μs structures are not significantly higher than those in the other structures, including the dark state structure (**Figure 8**).

Subunit L	$E_m(H_L)$	$E_m(H_M)$	Subunit M	$E_m(H_L)$	$E_m(H_M)$	Difference
Ala-L120	-4	0	Asn-M147	0	-42	38
Asp-L218	-2	-22	Trp-M252	1	0	20
Arg-L103	77	3	Arg-M130	3	59	17
Ala-L237	-2	0	Ser-M271	3	-16	16
Lys-L110	17	2	Ala-M137	0	3	14
Val-L219	1	5	Thr-M253	17	1	11
His-L211	1	0	Arg-M245	14	4	11

Table 2.

Contributions of the L/M residue pairs that are responsible for $E_m(H_L) > E_m(H_M)$ (more than 10 mV) in the dark-state structure (mV). Difference: [contribution of subunit L to $E_m(H_L)$] + [contribution of subunit M to $E_m(H_L)$] – [contribution of subunit L to $E_m(H_M)$] – [contribution of subunit M to $E_m(H_M)$].

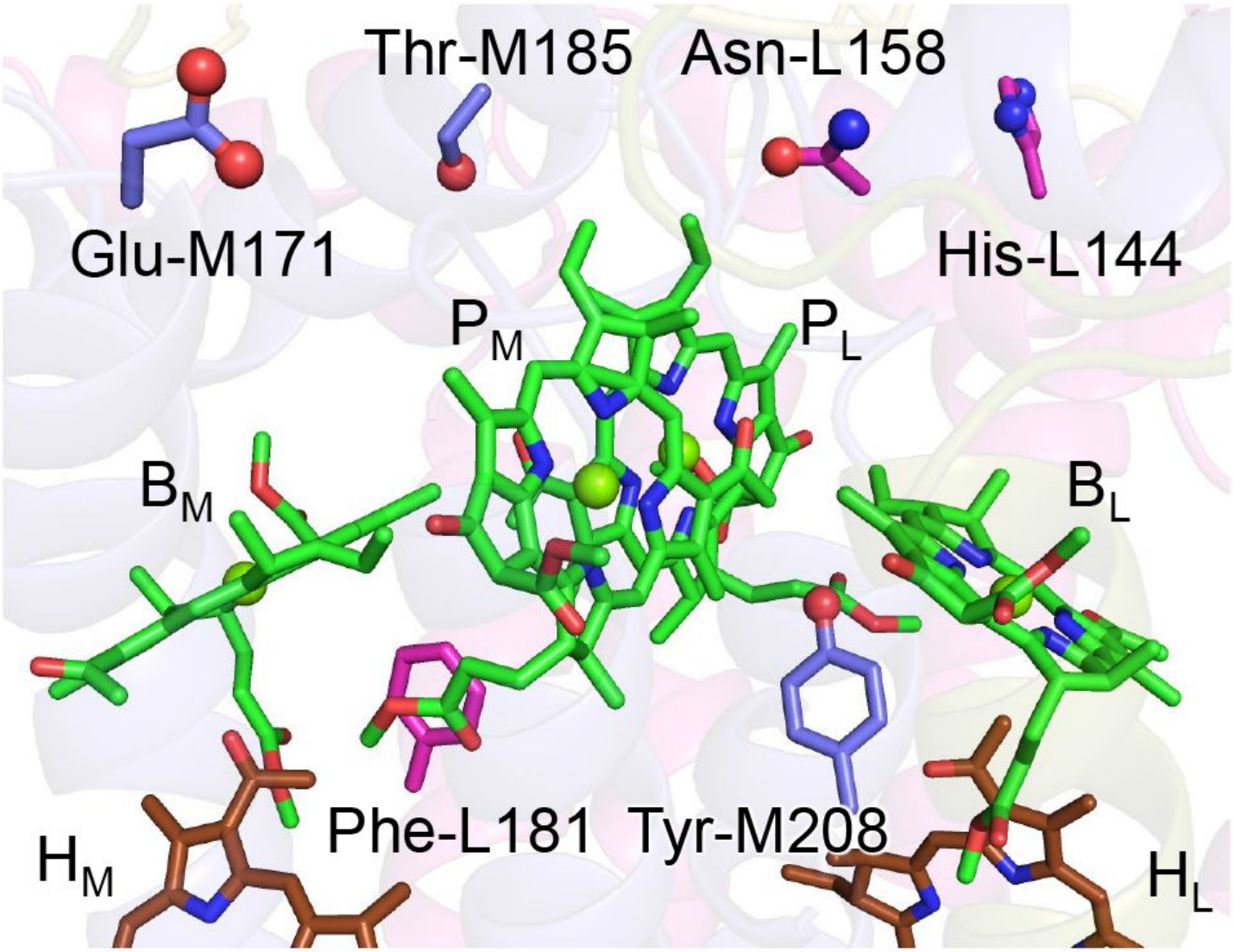

Figure 4.

Residue pairs that are responsible for $E_m(B_L) > E_m(B_M)$.

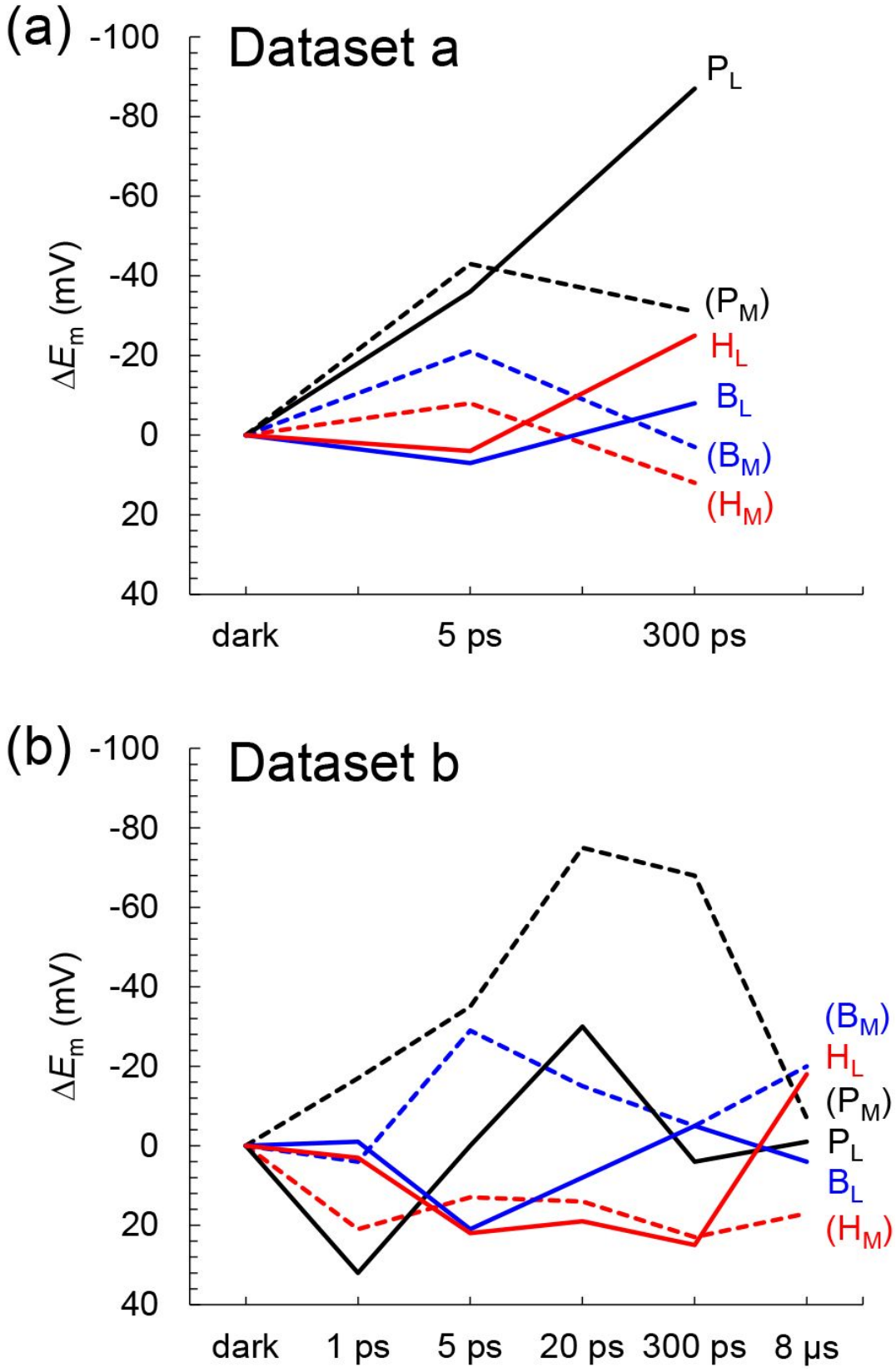

Figure 5.

Time-dependent E_m changes for BChl*b* and BPheo*b* in the XFEL structures. (a) Dataset a. (b) Dataset b. ΔE_m denotes the E_m shift with respect to the dark state structure. Black solid lines: P_L; black dotted lines: P_M; blue solid lines B_L; blue dotted lines: B_M; red solid lines: H_L; red dotted lines: H_M.

Dataset a		shift		shift
0 to 5 ps	Ser-L176	5	Cys-M210	4
	Thr-M220	-7	B_L	-5
5 to 300 ps	B_L	7	Gly-M209	3
	Gly-M211	-11	Leu-M212	-8

Table 3.

Residues that shift $E_m(H_L)$ most significantly during putative electron transfer in the XFEL structures (dataset a) (mV). The same residues are highlighted in the same colors for clarity.

Dataset b		shift		shift
0 to 1 ps	Ser-L238	8	Ser-L176	7
	B_L	-7	Leu-M213	-3
1 to 5 ps	Gly-M211	6	Leu-M213	5
	Ser-L238	-6	Thr-M253	-5
5 to 20 ps	B_L	12	Thr-M253	7
	Leu-M213	-4	P_M	-3
20 to 300 ps	Ser-L238	3	Gly-M211	2
	B_L	-10	Glu-L212	-4
300 ps to 8 μs	Glu-L212	4	Leu-M213	4
	B_L	-6	Gly-M211	-5

Table 4.

Residues that shift $E_m(H_L)$ most significantly during putative electron transfer in the XFEL structures (dataset b) (mV). The same residues are highlighted in the same colors for clarity.

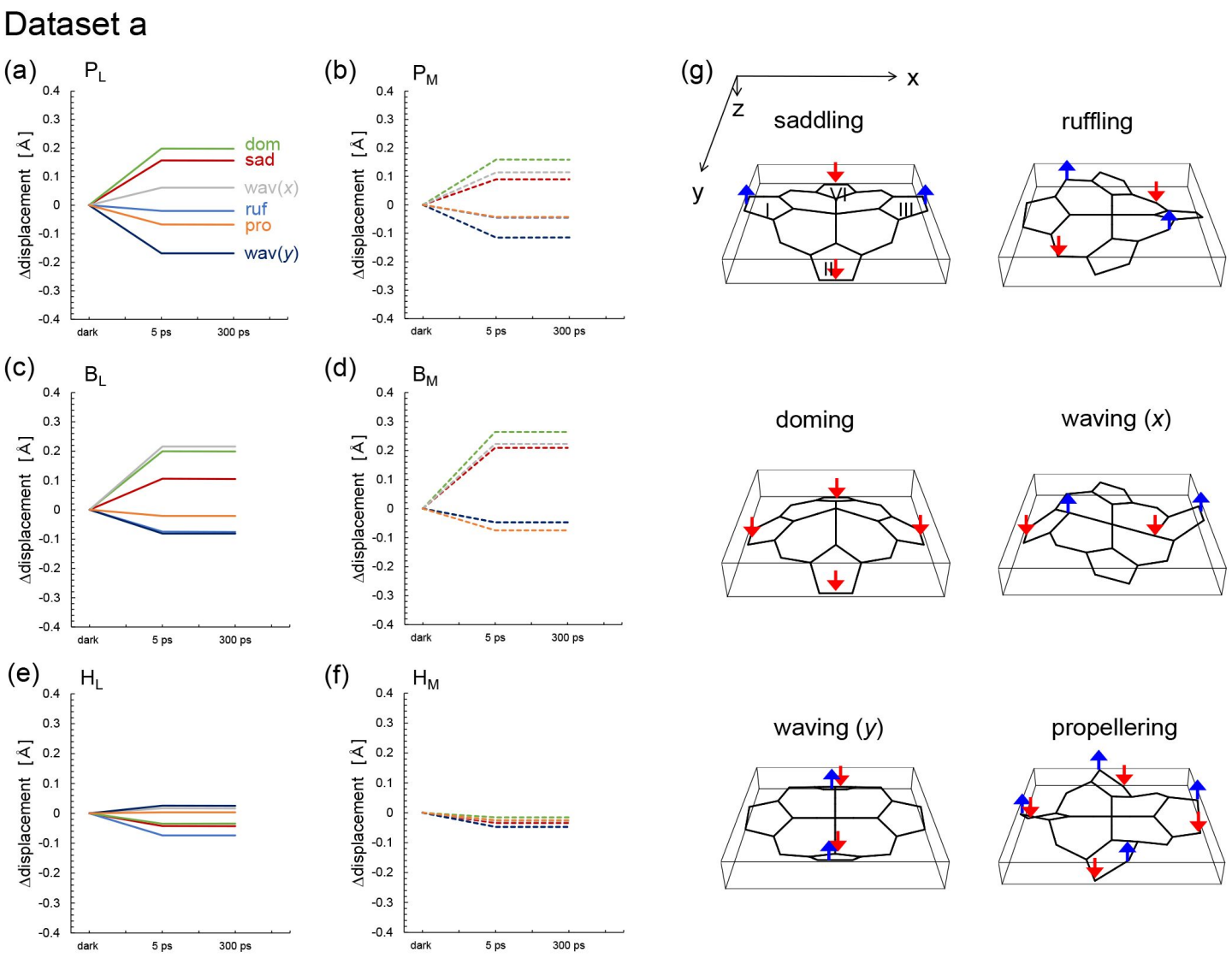

Figure 6.

Time-dependent changes in the lowest frequency out-of-plane modes of the chlorin rings in the XFEL structures (dataset a). Sad: saddling (red); ruf: ruffling (blue); dom: doming (green); wav(*x*, *y*): waving (*x*, *y*) (gray, dark blue); pro: propellering (orange). Solid and dotted lines indicate L and M branches, respectively. See Table S2 for the absolute values in the dark state for dataset a.

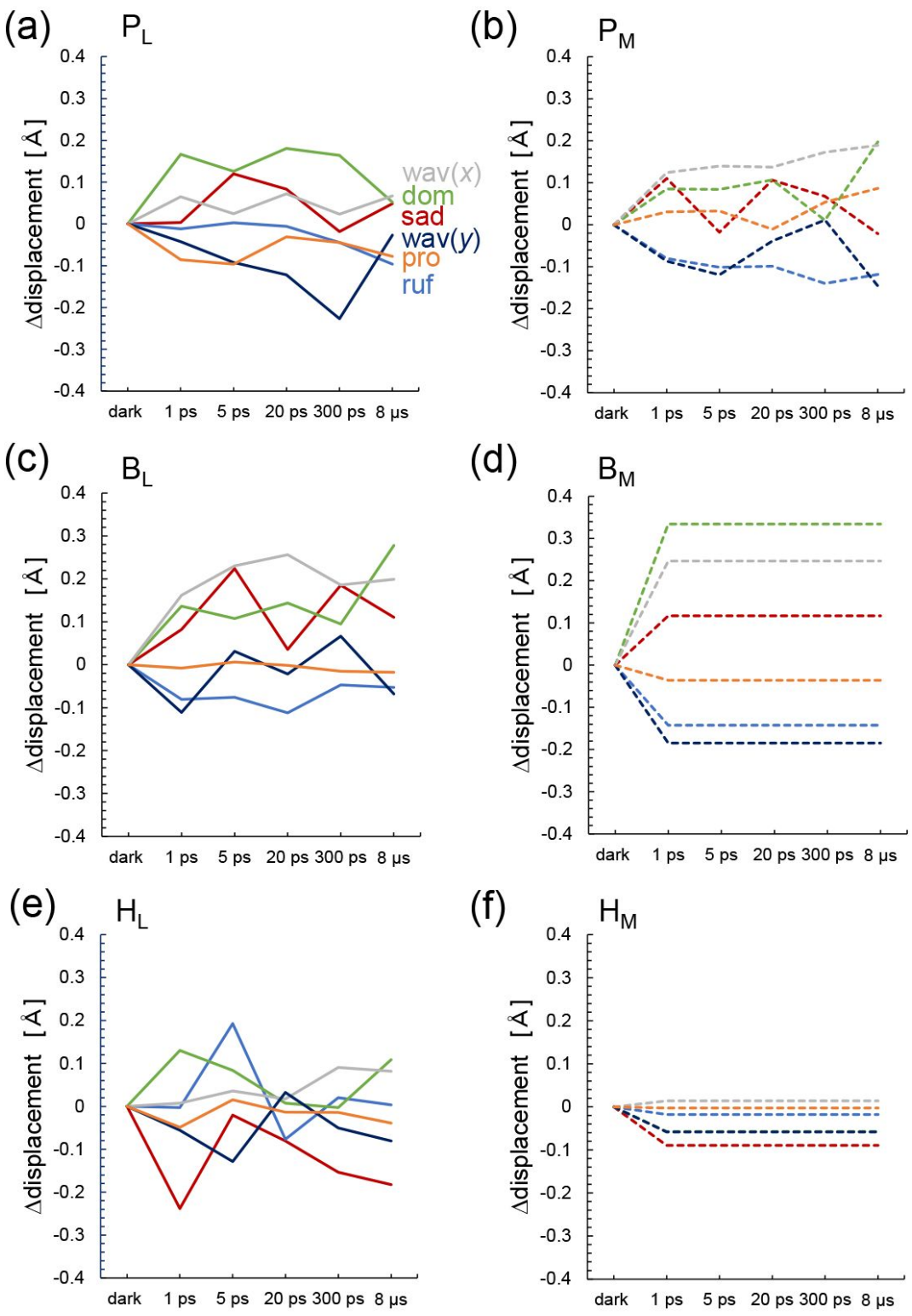

Figure 7.

Time-dependent changes in the lowest frequency out-of-plane modes of the chlorin rings in the XFEL structures (dataset b). Sad: saddling (red); ruf: ruffling (blue); dom: doming (green); wav(*x*, *y*): waving (*x*, *y*) (gray, dark blue); pro: propellering (orange). Solid and dotted lines indicate L and M branches, respectively. See Table S3 for the absolute values in the dark state for dataset b.

	saddling	ruffling	doming	waving		propellering
	B_{2u}	B_{1u}	A_{2u}	$E_{g(x)}$	$E_{g(y)}$	A_{1u}
H_L	0.18	0.35	-0.10	0.13	-0.11	0.13
$H_L^{\bullet-}$	0.24	0.35	-0.09	0.12	-0.12	0.13
$(P_L^{\bullet+}H_L^{\bullet-})$	(0.22)	(0.36)	(-0.07)	(0.13)	(-0.13)	(0.13)
$H_L/H_L^{\bullet-}$ difference	0.06	0.00	0.01	-0.01	-0.01	0.00
H_M	0.06	0.40	-0.20	0.37	0.12	0.19
$H_M^{\bullet-}$	0.12	0.38	-0.22	0.33	0.09	0.22
$(P_L^{\bullet+}H_M^{\bullet-})$	(0.14)	(0.38)	(-0.22)	(0.33)	(0.10)	(0.22)
$H_M/H_M^{\bullet-}$ difference	0.06	-0.02	-0.02	-0.04	-0.03	0.03

Table 5.

Induced out-of-plane distortion of H_L and H_M in the PbRC protein environment of the dark structure for dataset a in response to the reduction (Å).

	saddling	ruffling	doming	waving		propellering
	B_{2u}	B_{1u}	A_{2u}	$E_{g(x)}$	$E_{g(y)}$	A_{1u}
H_L	0.13	0.35	-0.13	0.07	-0.09	0.20
$H_L^{\bullet-}$	0.25	0.34	-0.02	0.12	-0.16	0.13
$(P_L^{\bullet+}H_L^{\bullet-})$	(0.23)	(0.34)	(-0.03)	(0.12)	(-0.16)	(0.12)
$H_L/H_L^{\bullet-}$ difference	0.12	-0.01	0.11	0.05	-0.07	-0.07
H_M	0.08	0.57	-0.11	0.16	0.20	0.32
$H_M^{\bullet-}$	0.16	0.36	-0.19	0.36	0.18	0.21
$(P_L^{\bullet+}H_M^{\bullet-})$	(0.16)	(0.36)	(-0.20)	(0.36)	(0.18)	(0.21)
$H_M/H_M^{\bullet-}$ difference	0.08	-0.21	-0.08	0.20	-0.02	-0.11

Table 6.

Induced out-of-plane distortion of H_L and H_M in the PbRC protein environment of the dark structure for dataset b in response to the reduction (Å).

Consequently, the lack of a clear relationship between the charge separated state and the changes in $E_m(Q_A)$ at 300 ps and 8-μs further strengthens the argument that the XFEL structures are irrelevant to the electron transfer events.

In summary, the E_m values in the active L branch are higher than those in the inactive M branch in the XFEL structures, which suggests that electron transfer via $B_L^{\bullet-}$ and $H_L^{\bullet-}$ is energetically more favored than that via $B_M^{\bullet-}$ and $H_M^{\bullet-}$ (**Figure 2**). The Phe-L181/Tyr-M208 pair contributes to the difference between $E_m(B_L)$ and $E_m(B_M)$ the most significantly, as observed in the Phe-L181/Tyr-M210 pair in PbRC from *Rhodobacter sphaeroides* [13, 28]. The stabilization of the $[P_LP_M]^{\bullet+}H_L^{\bullet-}$ state owing to protein reorganization is not clearly observed in the $E_m(H_L)$ values (**Figure 5**). The absence of the induced saddling mode in the H_L chlorin ring in the 5- and 20-ps structures suggests that $H_L^{\bullet-}$ does not specifically exist in these XFEL structures (**Figures 6** and **7**). The cyclic fluctuations in the contributions of the residues to $E_m(H_L)$ at different time intervals suggest that the structural differences among the XFEL structures are not related to the actual time course of charge separation (**Table 4**). The major limitation of the structural studies conducted by Dods et al. [8] is the relatively low resolution of their XFEL structures, primarily at 2.8 Å. Consequently, the observed changes in E_m values and chlorin ring deformations are more likely to reflect experimental errors rather than actual structural changes induced by electron transfer events. This concern is reinforced by the lack of a clear relationship between the actual $Q_A^{\bullet-}$ formation and the $E_m(Q_m)$ values in the 300-ps and 8-μs structures (**Figure 8**). Consequently, the proposed time-dependent structural changes proposed by Dods et al. [8] are highly likely irrelevant to the electron transfer events.

Hence, it is crucial to exercise caution when interpreting time-dependent XFEL structures, especially in the absence of comprehensive evaluations of the energetics and accompanying structural changes. This cautionary note should serve as a counterargument in the future, highlighting the potential pitfalls associated with presenting time-dependent XFEL structures of insufficient quality and drawing conclusive interpretations of protein structural changes that may not be distinguishable from significant experimental errors. Future high-resolution structures may provide further insights into the actual structural changes relevant to electron transfer events. By combining both high-resolution structures and rigorous energetic evaluations, a more comprehensive understanding of the protein structure-function relationship can be achieved.

Acknowledgements

This research was supported by JSPS KAKENHI (JP23H04963 to K.S.; JP20H03217 and JP23H02444 to H.I.) and Interdisciplinary Computational Science Program in CCS, University of Tsukuba.

Competing financial interests

The authors declare no financial and non-financial competing interests.

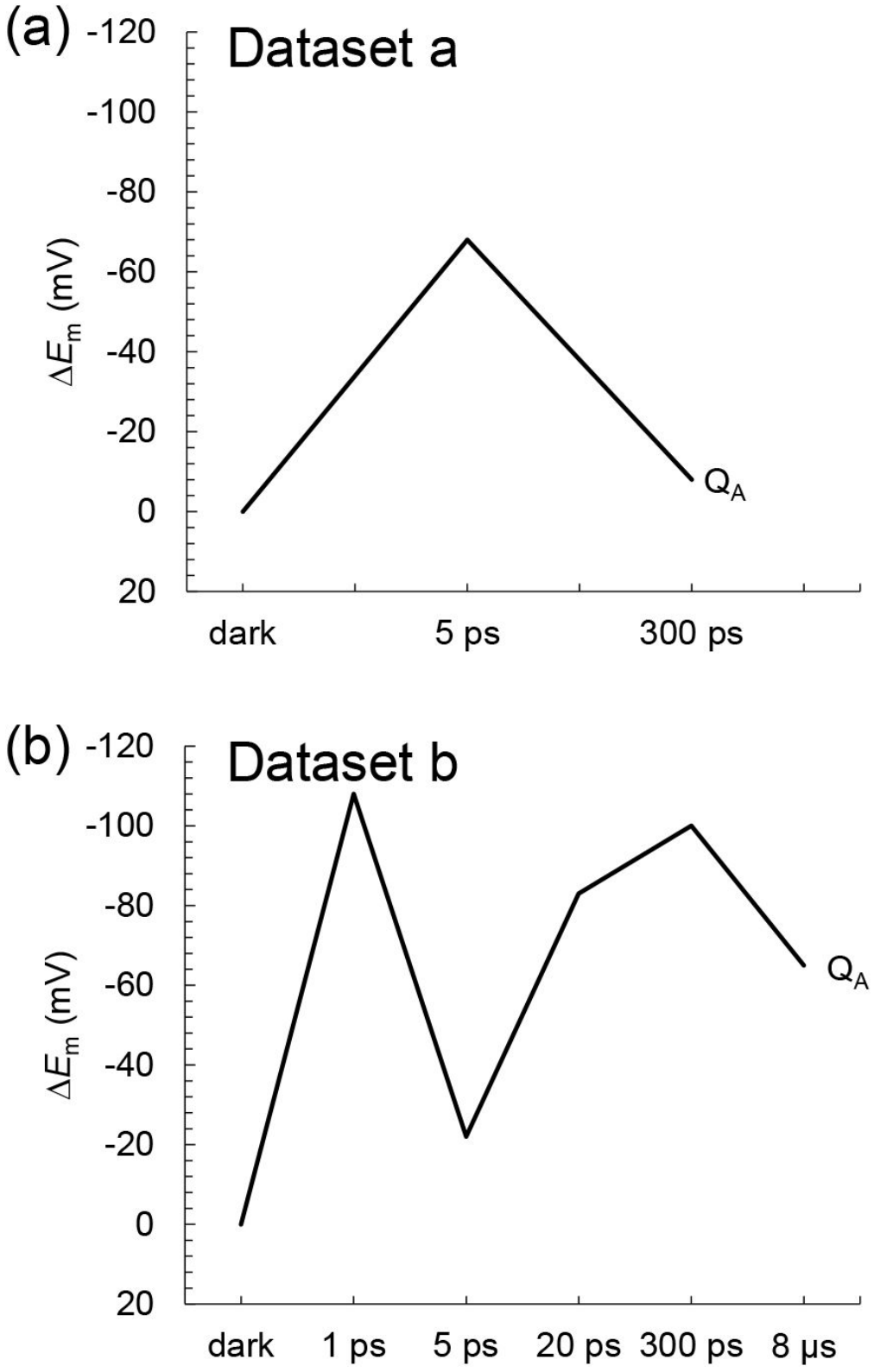

Figure 8.

Time-dependent E_m changes for Q_A in the XFEL structures. (a) Dataset a. (b) Dataset b. ΔE_m denotes the E_m shift with respect to the dark state structure. Note that the calculated $E_m(Q_A)$ values for dataset a and dataset b in the dark structure are –223 mV and –209 mV, respectively, which are comparable to experimentally measured values of –150 mV for PbRC from *Blastochloris viridis* (menaquinone) [29] and –180 mV for PbRC from *Rhodobacter sphaeroides* (ubiquinone) [30].

References

1. Deisenhofer J., Epp O., Miki K., Huber R., Michel H (1985) **Structure of the protein subunits in the photosynthetic reaction centre of Rhodopseudomonas viridis at 3 Å resolution** *Nature* **318**:618–624

2. Rabenstein B., Ullmann G. M., Knapp E.-W (1998) **Energetics of electron-transfer and protonation reactions of the quinones in the photosynthetic reaction center of Rhodopseudomonas viridis** *Biochemistry* **37**:2488–2495

3. Kirmaier C., Laible P. D., Hanson D. K., Holten D (2003) **B-side charge separation in bacterial photosynthetic reaction centers: nanosecond time scale electron transfer from HB- to QB** *Biochemistry* **42**:2016–2024

4. Holzapfel W., Finkele U., Kaiser W., Oesterhelt D., Scheer H., Stilz H. U., Zinth W (1990) **Initial electron-transfer in the reaction center from Rhodobacter sphaeroides** *Proc Natl Acad Sci U S A* **87**:5168–5172

5. Marcus R. A., Sutin N (1985) **Electron transfers in chemistry and biology** *Biochim. Biophys. Acta* **811**:265–322

6. Saito K., Umena Y., Kawakami K., Shen J. R., Kamiya N., Ishikita H (2012) **Deformation of chlorin rings in the photosystem II crystal structure** *Biochemistry* **51**:4290–4299

7. Müh F., Williams J. C., Allen J. P., Lubitz W (1998) **A conformational change of the photoactive bacteriopheophytin in reaction centers from Rhodobacter sphaeroides** *Biochemistry* **37**:13066–13074

8. Dods R., Båth P., Morozov D., Gagnér V. A., Arnlund D., Luk H. L., Kübel J., Maj M., Vallejos A., Wickstrand C., Bosman R., Beyerlein K. R., Nelson G., Liang M., Milathianaki D., Robinson J., Harimoorthy R., Berntsen P., Malmerberg E., Johansson L., Andersson R., Carbajo S., Claesson E., Conrad C. E., Dahl P., Hammarin G., Hunter M. S., Li C., Lisova S., Royant A., Safari C., Sharma A., Williams G. J., Yefanov O., Westenhoff S., Davidsson J., DePonte D. P., Boutet S., Barty A., Katona G., Groenhof G., Brändén G., Neutze R (2021) **Ultrafast structural changes within a photosynthetic reaction centre** *Nature* **589**:310–314

9. Jentzen W., Song X.-Z., Shelnutt J. A (1997) **Structural characterization of synthetic and protein-bound porphyrins in terms of the lowest-frequency normal coordinates of the macrocycle** *J Phys Chem B* **101**:1684–1699

10. Shelnutt J. A., Song X.-Z., Ma J.-G., Jia S.-L., Jentzen W., Medforth C. J (1998) **Nonplanar porphyrins and their significance in proteins** *Chem Soc Rev* **27**:31–41

11. Brooks B. R., Bruccoleri R. E., Olafson B. D., States D. J., Swaminathan S., Karplus M (1983) **CHARMM: a program for macromolecular energy minimization and dynamics calculations** *J. Comput. Chem* **4**:187–217

12. MacKerell A. D., Bashford D., Bellott R. L., Dunbrack R. L., Evanseck J. D., Field M. J., Fischer S., Gao J., Guo H., Ha S., Joseph-McCarthy D., Kuchnir L., Kuczera K., Lau F. T. K., Mattos C., Michnick S., Ngo T., Nguyen D. T., Prodhom B., Reiher W. E., Roux III, Schlenkrich B., Smith M., Stote J. C., Straub R., Watanabe J., Wiorkiewicz-Kuczera M., Yin J., Karplus D. (1998) **All-atom empirical potential for molecular modeling and dynamics studies of proteins** *J. Phys. Chem. B* **102**:3586–3616

13. Kawashima K., Ishikita H (2018) **Energetic insights into two electron transfer pathways in light-driven energy-converting enzymes** *Chem Sci* **9**:4083–4092

14. Kawashima K., Ishikita H (2017) **Structural factors that alter the redox potential of quinones in cyanobacterial and plant photosystem I** *Biochemistry* **56**:3019–3028

15. Bayly C. I., Cieplak P., Cornell W. D., Kollman P. A (1993) **A well-behaved electrostatic potential based method using charge restraints for deriving atomic charges: the RESP model** *J. Phys. Chem* **97**:10269–10280

16. Jaguar (2012) **version 7.9**

17. Bashford D., Karplus M (1990) **Pkas of Ionizable Groups in Proteins - Atomic Detail from a Continuum Electrostatic Model** *Biochemistry* **29**:10219–10225

18. Fajer J., Davis M. S., Brune D. C., Spaulding L. D., Borg D. C., Forman A (1976) **Chlorophyll radicals and primary events** *Brookhaven Symp. Biol* **28**

19. Watanabe T., Kobayashi M., Scheer H. (1991) **Electrochemistry of chlorophylls** *in Chlorophylls* :287–303

20. Kishi S., Saito K., Kato Y., Ishikita H (2017) **Redox potentials of ubiquinone, menaquinone, phylloquinone, and plastoquinone in aqueous solution** *Photosynth Res* **134**:193–200

21. Rabenstein B., Knapp E. W (2001) **Calculated pH-dependent population and protonation of carbon-monoxy-myoglobin conformers** *Biophys. J* **80**:1141–1150

22. QSite (2012) **version 5.8**

23. Humphrey W., Dalke A., Schulten K (1996) **VMD: Visual molecular dynamics** *Journal of Molecular Graphics* **14**:33–38

24. Zucchelli G., Brogioli D., Casazza A. P., Garlaschi F. M., Jennings R. C (2007) **Chlorophyll ring deformation modulates Qy electronic energy in chlorophyll-protein complexes and generates spectral forms** *Biophys J* **93**:2240–2254

25. Tamura H., Saito K., Ishikita H (2020) **Acquirement of water-splitting ability and alteration of the charge-separation mechanism in photosynthetic reaction centers** *Proc Natl Acad Sci U S A* **117**:16373–16382

26. Rutherford A. W., Heathcote P., Evans M. C. W (1979) **Electron-paramagnetic-resonance measurements of the electron-transfer components of the reaction centre of Rhodopseudomonas viridis. Oxidation–reduction potentials and interactions of the electron acceptors** *Biochemical Journal* **182**:515–523

27. Gunner M. R., Nicholls A., Honig B (1996) **Electrostatic potentials in Rhodopseudomonas viridis reaction centers: implications for the driving force and directionality of electron transfer** *J. Phys. Chem* **100**:4277–4291

28. Parson W. W., Chu Z.-T., Warshel A (1990) **Electrostatic control of charge separation in bacterial photosynthesis** *Biochim. Biophys. Acta* **1017**:251–272

29. Prince R. C., Leigh J. S., Dutton P. L (1976) **Thermodynamic properties of the reaction center of Rhodopseudomonas viridis in vivo measurement of the reaction center bacteriochlorophyll-primary acceptor intermediary electron carrier** *Biochim. Biophys. Acta* **440**:622–636

30. Prince R. C., Dutton P. L (1976) **The primary acceptor of bacterial photosynthesis: its operating midpoint potential?** *Arch. Biochem. Biophys* **172**:329–334

Author information

Gai Nishikawa
Department of Applied Chemistry, The University of Tokyo, 7-3-1 Hongo, Bunkyo-ku, Tokyo 113-8654, Japan

Yu Sugo
Department of Applied Chemistry, The University of Tokyo, 7-3-1 Hongo, Bunkyo-ku, Tokyo 113-8654, Japan
ORCID iD: 0000-0001-8123-1895

Keisuke Saito
Department of Applied Chemistry, The University of Tokyo, 7-3-1 Hongo, Bunkyo-ku, Tokyo 113-8654, Japan, Research Center for Advanced Science and Technology, The University of Tokyo, 4-6-1 Komaba, Meguro-ku, Tokyo 153-8904, Japan
ORCID iD: 0000-0002-2293-9743

Hiroshi Ishikita
Department of Applied Chemistry, The University of Tokyo, 7-3-1 Hongo, Bunkyo-ku, Tokyo 113-8654, Japan, Research Center for Advanced Science and Technology, The University of Tokyo, 4-6-1 Komaba, Meguro-ku, Tokyo 153-8904, Japan
For correspondence: hiro@appchem.t.u-tokyo.ac.jp
ORCID iD: 0000-0002-5849-8150

Editors

Reviewing Editor
Volker Dötsch
Goethe University, Germany

Senior Editor
Volker Dötsch
Goethe University, Germany

Reviewer #1 (Public Review):

First, I agree with the authors of this manuscript that conformational changes in the XFEL structures with 2.8 A resolution are not reliable enough for demonstrating the subtle changes in the electron transfer events in this bacterial photosynthesis system. Actually, the data statistics in the paper by Dods et al. showed that the high-resolution range of some of the XFEL datasets may include pretty high noise (low CC1/2 and high Rsplit) so the comparison of the subtle conformational changes of the structures is problematic.

The manuscript by Gai Nishikawa investigated time-dependent changes in the energetics of the electron transfer pathway based on the structures by Dods et al. by calculating redox potential of the active and inactive branches in the structures and found no clear link between the time-dependent structural changes and the electron transfer events in the XFEL structures published by Dods, R.et al. (2021). This study provided validation for the interpretation of the structures of those electron-transferring proteins.

The paper was well prepared.

Comments on latest version:

The revisions the authors have made have improved the manuscript.

Reviewer #2 (Public Review):

The manuscript by Nishikawa et al. addresses time-dependent changes in the electron transfer energetics in the photosynthetic reaction center from Blastochloris viridis, whose time-dependent structural changes upon light illumination were recently demonstrated by time-resolved serial femtosecond crystallography (SFX) using X-ray free-electron laser (XFEL) (Dods et al., Nature, 2021). Based on the redox potential Em values of bacteriopheophytin in the electron transfer active branch (BL) by solving the linear Poisson-Boltzmann equation, the authors found that Em(HL) values in the charge-separated 5-ps structure obtained by XFEL are not clearly changed, suggesting that the P+HL- state is not stabilized owing to protein reorganization. Furthermore, chlorin ring deformation upon HL- formation, which was expected from their QM/MM calculation, is not recognized in the 5-ps XFEL structure. Then the authors concluded that the structural changes in the XFEL structures are not related to the actual time course of charge separation. They argued that their calculated changes in Em and chlorin ring deformations using the XEFL structures may reflect the experimental errors rather than the real structural changes; they mentioned this problem is due to the fact that the XFEL structures were obtained at not high resolutions (mostly at 2.8 Å). I consider that their systematic calculations may suggest a useful theoretical interpretation of the XFEL study.

Comments on latest version:

The authors have satisfied my concerns. I consider that their present manuscript is more attractive and informative for readers.

Author Response

The following is the authors' response to the previous reviews.

Reviewer #1 Public Review

"First, I agree with the authors of this manuscript that conformational changes in the XFEL structures with 2.8 A resolution are not reliable enough for demonstrating the subtle changes in the electron transfer events in this bacterial photosynthesis system. Actually, the data statistics in the paper by Dods et al. showed that the high-resolution range of some of the XFEL datasets may include pretty high noise (low CC1/2 and high Rsplit) so the comparison of the subtle conformational changes of the structures is problematic.

The manuscript by Gai Nishikawa investigated time-dependent changes in the energetics of the electron transfer pathway based on the structures by Dods et al. by calculating redox potential of the active and inactive branches in the structures and found no clear link between the time-dependent structural changes and the electron transfer events in the XFEL structures published by Dods, R.et al. (2021). This study provided validation for the interpretation of the structures of those electrontransferring proteins.

The paper was well prepared."

Thank you very much for your positive and insightful comment. We greatly appreciate your suggestion regarding the high noise levels of the XFEL structures. Including this information in the Introduction section will draw readers' attention to the concerns about the reliability of these XFEL structures. We have incorporated it into the Introduction section.

Reviewer #2 Public Review

"The manuscript by Nishikawa et al. addresses time-dependent changes in the electron transfer energetics in the photosynthetic reaction center from Blastochloris viridis, whose time-dependent structural changes upon light illumination were recently demonstrated by time-resolved serial femtosecond crystallography (SFX) using X-ray free-electron laser (XFEL) (Dods et al., Nature, 2021). Based on the redox potential Em values of bacteriopheophytin in the electron transfer active branch (BL) by solving the linear Poisson-Boltzmann equation, the authors found that Em(HL) values in the charge-separated 5-ps structure obtained by XFEL are not clearly changed, suggesting that the P+HL- state is not stabilized owing to protein reorganization. Furthermore, chlorin ring deformation upon HL- formation, which was expected from their QM/MM calculation, is not recognized in the 5ps XFEL structure. Then the authors concluded that the structural changes in the XFEL structures are not related to the actual time course of charge separation. They argued that their calculated changes in Em and chlorin ring deformations using the XEFL structures may reflect the experimental errors rather than the real structural changes; they mentioned this problem is due to the fact that the XFEL structures were obtained at not high resolutions (mostly at 2.8 Å). I consider that their systematic calculations may suggest a useful theoretical interpretation of the XFEL study. However, the present manuscript insists as a whole negatively that the experimental errors may hamper to provide the actual structural changes relevant to the electron transfer events."

Thank you for your feedback on our manuscript. We appreciate your positive assessment of our systematic calculations and theoretical interpretation of the XFEL study. We have carefully considered your comments and made the necessary revisions to address your concerns.

Reviewer #2 Recommendations for the authors

"The authors have satisfied my concerns mostly, in particular by providing the Em(QA) changes, which seem to be more attractive in the present form. However, the Em(QA) value(s), at least in the dark structure, should be provided, and the procedure of the calculation for the Em(QA) value(s) should be described in METHODS "Calculation of Em".

The calculated Em(QA) values for dataset a and dataset b in the dark structure are –223 mV and – 209 mV, respectively, using the reference Em value of –256 mV versus NHE for menaquinone-2 in water [Photosynth. Res. 134 (2017) 193]. These calculated values are comparable to experimentally measured values of –150 mV for PbRC from Blastochloris viridis (naphtoquinone) [Biochim. Biophys. Acta 440 (1976) 622] and –180 mV for PbRC from Rhodobacter sphaeroides (ubiquinone) [Arch. Biochem. Biophys 172 (1976) 329].

We have now provided this information in the Method ("Calculation of Em") and Results and Discussion ("Relevance of structural changes observed in XFEL structures") sections.